An evaluation of the C/N ratio of the mantle from natural CO_2-rich gas analysis: Geochemical and cosmochemical implications

Bernard Marty[1*], Matthieu Almayrac[1], Peter H. Barry[2], David V. Bekaert[1,2], Michael W. Broadley[1], David J. Byrne[1], Christopher J. Ballentine[3] and Antonio Caracausi[4]

[1]Université de Lorraine, CNRS, CRPG, F-54000 Nancy, France

[2]Marine Chemistry and Geochemistry Dept., Woods Hole Oceanographic Institution, Woods Hole, MA 02543, USA

[3]Department of Earth Sciences, University of Oxford, OX1 3AN Oxford, United Kingdom

[4]Instituto Nazionale di Geofisica e Vulcanologia, Sezione di Palermo, 90146 Palermo, Italy

*Corresponding author - Email: bernard.marty@univ-lorraine.fr

Abstract

The terrestrial carbon to nitrogen ratio is a key geochemical parameter that can provide information on the nature of Earth's precursors, accretion/differentiation processes of our planet, as well as on the volatile budget of Earth. In principle, this ratio can be determined from the analysis of volatile elements trapped in mantle-derived rocks like mid-ocean ridge basalts (MORB), corrected for fractional degassing during eruption. However, this correction is critical and previous attempts have adopted different approaches which led to contrasting *C/N* estimates for the bulk silicate Earth (BSE) (Marty and Zimmermann, 1999; Bergin et al., 2015). Here we consider the analysis of CO_2-rich gases worldwide for which a mantle origin has been determined using noble gas isotopes in order to evaluate the *C/N* ratio of the mantle source regions. These gases experienced little fractionation due to degassing, as indicated by radiogenic $^{4}He/^{40}Ar^{*}$ values (where ^{4}He and ^{40}Ar* are produced by the decay of U+Th, and ^{40}K isotopes, respectively) close to the mantle production/accumulation values. The *C/N* and $C/^{3}He$ ratios of gases investigated here are within the range of values previously observed in oceanic basalts. They point to an elevated mantle *C/N* ratio (~350-470, molar) higher than those of potential cosmochemical accretionary endmembers. For example, the BSE *C/N* and $^{36}Ar/N$ ratios (160-220 and 75 x 10^{-7}, respectively) are higher than those of CM-CI chondrites but within the range of CV-CO groups. This similarity suggests that the Earth accreted from evolved planetary precursors depleted in volatile and moderately volatile elements. Hence the high *C/N* composition of the BSE may be an inherited feature rather than the result of terrestrial differentiation. The *C/N* and $^{36}Ar/N$ ratios of the surface (atmosphere plus crust) and of the mantle cannot be easily linked to any known chondritic composition. However, these compositions are consistent with early sequestration of carbon into the mantle (but not N and noble gases), permitting the establishment of clement temperatures at the surface of our planet.

1. Introduction

Carbon and nitrogen are essential ingredients to build a habitable Earth-like planet (Alexander et al., 2012; Marty, 2012; Bergin et al., 2015; Johnson and Goldblatt, 2015; Hirschmann, 2018; Grewal et al., 2020). Together with water, these elements were delivered to Earth by accretionary materials mainly originating from the inner solar system, whose remnants can be found in primitive meteorites (chondrites). Stable isotope ratios point to an asteroidal-like origin for terrestrial water, carbon and nitrogen (Marty, 2012; Alexander et al., 2012), whereas other potential cosmochemical sources such as cometary material were likely to be minor (Bekaert et al., 2020). Of particular interest is C, one of the main greenhouse forcing elements in the atmosphere. Its present-day abundance at Earth's surface is reasonably well known from the geological record (27±5 ppmw, normalized to the mass of the BSE, 4.0 x 10^{27}g; Hirschmann, 2018), but the abundance of carbon in the other major terrestrial reservoirs (e.g., the core and the mantle) is not well-constrained and somewhat model-dependent (Dalou et al., 2017; Hirschmann, 2018; Grewal et al, 2020). For example, C is often advocated to be an important trace element in the core, but quantitative estimates of its concentration depend on several poorly constrained parameters such as pressure, composition-dependent metal-silicate partitioning coefficients and chronology of core formation (e.g., Dalou et al., 2017; Li et al., 2020). As both carbon and nitrogen are incompatible during partial melting under present-day mantle oxygen fugacity conditions, their contents in the mantle-derived lavas can thus, in principle, be used to estimate the composition of the mantle source. However, CO_2, the main carbon-bearing species in present-day magmas, has a low solubility in basaltic melts and lavas reaching Earth's surface are readily degassed, including those erupted at high hydrostatic pressure and rapidly quenched on the ocean floor. Some authors have considered oceanic basalt glasses with minimally-

degassed basalts (Hirschmann, 2018) to estimate the ratio of CO_2 to non-volatile elements with known geochemical behaviors such as Ba or Nd (Rosenthal et al., 2015), for which the mantle abundance are known. Assuming that the CO_2/Ba ratio (100±20 ppmw/ppmw; (Hirschmann, 2018) is representative of the mantle sources of analyzed lavas, and taking a Ba concentration of the convective mantle to be 4.0±0.4 ppmw (Palme and O'Neill, 2013), the concentration of C in the mantle was hence estimated at 110±40 ppmw for parent reservoirs (Hirschmann, 2018). Volcanism at the Earth's surface is volumetrically dominated by mid ocean ridge (MOR) magmatism (~16 km^3/yr; Le Voyer et al., 2019) which is sourced directly from the convecting depleted MORB mantle (DMM). The DMM carbon concentration can be estimated independently from the total flux of CO_2 from ridges, the magma production rate, and the average MOR melting rate (~12%). MOR CO_2 flux values computed following different approaches yield comparable values: [1.3±0.8] x 10^{12} mol/yr from MOR data compilation (Le Voyer et al., 2019), [2.2±0.9] x 10^{12} mol/yr (Marty and Tolstikhin, 1998) and [1.6±0.2] x 10^{12} mol/yr (Tucker et al., 2018) from calibration to ^{3}He. The corresponding MOR mantle C content would be about 20-30 ppmw (Tucker et al., 2018), significantly lower than the one obtained from the Ba calibration. Current constraints on the C content of the mantle therefore remain uncertain, especially if regions that are not involved in mantle convection (e.g., the plume mantle source) are significant repositories for C, as independently suggested by noble gas isotopes (e.g., Mukhopadhyay and Parai, 2019).

Nitrogen in the atmosphere-mantle system can be estimated on a global scale. N_2 and radiogenic ^{40}Ar abundances correlate in MORB glasses and ocean island basalt (OIB) glasses from different localities worldwide (Marty and Zimmermann, 1999; Marty and Dauphas, 2003). Consequently, the N content of the mantle can be estimated from that of ^{40}Ar produced by the decay of ^{40}K because the potassium content of the BSE is reasonably well estimated

(280±60 ppm K, Arevalo et al., 2009). Terrestrial ^{40}Ar has been produced by the radioactive decay of ^{40}K in the BSE, and about half (42^{+32}_{-18} %) of radiogenic ^{40}Ar (noted $^{40}Ar^*$) is now in the atmosphere as a result of terrestrial degassing (Allègre et al., 1996). The surface reservoirs (atmosphere: 0.97 ppmw N, sediments and crust) can account for about 1.56±0.06 ppmw N (Johnson and Goldblatt, 2015; Hirschmann, 2018; after correction in error propagation). Using a mass balance approach, the mantle N concentration was estimated to be around 1 ppmw (Marty, 2012) and more recently to be 1.10±0.55 ppmw (Hirschmann, 2018). Available constraints on the global inventory of N in the Earth's mantle and surface constitute a solid basis for estimating the volatile content of the BSE (Marty, 2012; Johnson and Goldblatt, 2015; Bergin et al., 2015; Hirschmann, 2018).

By combining the mantle carbon concentration obtained from calibration to Ba together with the above mantle N concentration, Bergin et al. (2015) estimated a mantle *C/N* ratio of ~90 (in the following elemental ratios are molar and written in italics while C and N concentrations are in ppmw of the BSE having a mass of 4 x 10^{27}g). Using their estimated surface *C/N* ratio (21±6), Bergin et al. proposed a BSE *C/N* ratio of 61±23. In contrast, Marty (2012) estimated a significantly higher BSE *C/N* ratio of 365±233 from the analysis of CO_2 and N_2 in MORBs and OIBs (Marty and Zimmermann, 1999; Marty and Dauphas, 2003). The implications are not trivial, as a high *C/N* ratio of the BSE would imply a high mantle C concentration and drastic volatile fractionation either in the planetesimals that formed our planet or during Earth's formation.

The bulk mantle *C/N* estimate of Marty (2012) is based on the C-N-noble gases composition of a suite of 47 MORB and OIB samples extracted following vacuum crushing to remove secondary contributions within basaltic glasses. Gases trapped in oceanic glasses always

constitute a residual fraction of the initial volatile content due to pre-eruption and syn-eruption degassing. Hence residual volatiles are elementally fractionated according to their solubilities in basaltic melts. The solubilities of N_2 and Ar are comparable ($K_{N2} \sim K_{Ar} \sim$ 2-3 x 10^{-12} mol/g.hPa; Jambon et al., 1985; Libourel et al., 2003), and their degassing fractionation is minimal. However, CO_2 and He are ~3 and ~10 times more soluble than N_2 or Ar respectively (K_{CO2} = 9 x 10^{-12} mol/g.hPa, Dixon et al., 1995; K_{He} = 2.5 x 10^{-11} mol/g.hPa, Jambon et al., 1985). Accordingly, He and CO_2 will be depleted (relative to N_2-Ar) in the first fractions of gas escaping from a magma and enriched in residual gas trapped in erupted lavas. One way to correct for degassing fractionation is to use the radiogenic $^4He/^{40}Ar^*$ ratio (where $^{40}Ar^*$ is the amount of ^{40}Ar corrected for atmospheric contamination). Its production/accumulation ratio in the mantle is estimated from the parent *(U+Th)/ K* abundance ratio to be ~2 (range: 1.8-3.0; e.g., Marty, 2012; Mukhopadhyay and Parai, 2019). Oceanic basalt glasses present systematically higher values in the range 3-96 (Marty and Zimmermann, 1999), demonstrating the effect of elemental fractionation that could be modeled following a Raleigh-type distillation process. The initial $(C/N)_i$ ratio of the mantle source could be computed from the measured $(C/N)_{meas}$ ratio according to *Eqn. 1*:

$$(C/N)_i = (C/N)_m \times \left[\frac{\left(^4He/^{40}Ar\right)_m}{\left(^4He/^{40}Ar\right)_i}\right]^{\left[\frac{\left(K_{N_2}^{-1}-K_{CO_2}^{-1}\right)}{\left(K_{He}^{-1}-K_{Ar}^{-1}\right)}\right]} \quad (1)$$

where K_j are the basaltic melt/gas partition coefficients for species *j* and suffixes *i* and *m* mean initial and measured, respectively. After correction, the mean MORB *(C/N)* ratio was computed to be 535±224 (Marty and Zimmermann, 1999), with E-MORBs (*(C/N)* = 1839±641) being richer in C (relative to N) than N-MORBs (*(C/N)* = 273±106). This study indicated that (i) the *C/N* ratio of the MORB mantle is much higher than that of the surface

inventory ($(C/N)_{surface}$ = 21±6, computed with abundances given in Hirchsmann, 2018), and (ii) the C content of mantle sources is highly variable, possibly due to preferential subduction of C compared to N (Marty and Zimmermann, 1999).

Bergin et al. (2015) questioned this approach by noting that the extent of correction for largely variable C/N ratios in MORB complicates the reconstruction of the *C/N* ratio of mantle sources (Bergin et al, 2015). Natural CO_2-rich gases for which isotopic ratios of C, N and noble gases demonstrate a mantle origin may provide an independent means to investigate the *C/N* ratio of the mantle. Continental CO_2-rich gases tap into large crustal volumes where mantle-derived gases have accumulated over long periods of time (Ballentine and Holland, 2008), making them presumably more representative of the original mantle composition than residual gases left over in oceanic basaltic glasses. Atmospheric and/or crustal contamination can be problematic for natural gases, yet the noble gases along with C and N can provide sensitive tools to assess these effects and identify the original mantle source composition. Here we have selected CO_2-rich gases from different geodynamic environments where these effects can be robustly corrected for, to thoroughly estimate the *C/N* ratios of the corresponding magma sources and provide new insights into the *C/N* ratio of the BSE.

2. Samples

We have selected CO_2-rich gases for which the $^{40}Ar/^{36}Ar$ ratios are markedly higher than the atmospheric value of 298.6. Other noble gas constraints were used as additional sample selection criteria, namely those with (i) mantle-derived helium, rich in primordial ^{3}He, (ii) mantle-derived neon with 3-isotope compositions lying along the MORB or the mantle plume

correlation, and (iii) excess ^{129}Xe from the radioactive decay of extinct ^{129}I (as mantle Xe is enriched in ^{129}Xe with respect to atmospheric Xe) (*Table 1*). Samples having all these features are not common and as far as we know are restricted to the list presented in *Table 1*.

We include CO_2-rich gases from continental Europe. Bräuer et al.(2013) carried out a systematic survey of CO_2-rich gases in the Eifel quaternary volcanic province (Germany), and found two locations (Victoriaquelle and Schwefelquelle) with elevated $^{40}Ar/^{36}Ar$ ratios in the range 1,500-3,000. Repeated sampling of these springs by the CRPG group identified even higher $^{40}Ar/^{36}Ar$ ratios up to 8,300, ^{129}Xe excesses up to 7 % relative to atmospheric Xe and MORB-like neon (Bekaert et al., 2019). Nitrogen isotopologues of these samples indicate undetectable atmospheric N_2 contribution (Labidi et al., 2020). We also include data for a CO_2-rich gas sampled at Bublak, Eger graben, Czech Republic (Bräuer et al., 2004).

In 2018, we undertook a survey of geothermal gases in the Yellowstone National Park (USA), which is located at the present-day apex of a high-^{3}He mantle plume (Craig et al., 1978). Some of the gases that were collected show $^{40}Ar/^{36}Ar$ ratios higher than the atmospheric value (Broadley et al., 2020) and their data are reported here in three groups (*Table 1*): (i) the Mud Volcano group located inside the Yellowstone caldera where the highest $^3He/^4He$ values ($\geq$ 14 Ra, typical of mantle plume He signature) are observed (Craig et al., 1978); (ii) the Turbid Lake group located at the border of the caldera ($^3He/^4He$ = 5.2 Ra), and (iii) the Brimstone Basin group outside the caldera ($^3He/^4He$ = 2.8 Ra). He isotope variations are consistent with dilution of a typical mantle plume signature by radiogenic He from the Precambrian basement. Brimstone Basin samples also have Xe and Ne isotopes consistent with a crustal contribution to plume-like noble gases (Broadley et al., 2020). Nitrogen isotopologues of Yellowstone

gases also point to a mantle plume origin for nitrogen, with limited contributions of atmospheric or crustal N (Labidi et al., 2020).

The Naftia sample from Sicily is a CO_2 well gas in the vicinity of Mount Etna which shows an excess of ^{129}Xe and MORB-like Ne (Nakai et al., 1997). At this site, the $^{3}He/^{4}He$ ratio varies between 6 and 7 Ra and correlates with the eruptive activity at Mt. Etna, suggesting that new injections of magma under the volcano periodically contribute fresh mantle gases to this CO_2 reservoir (Caracausi et al., 2003). Volcanic gases were also sampled at Oldoinyo Lengai, an active carbonatitic volcano located on the eastern branch of the East African Rift Valley (Fischer et al., 2009). Atmospheric contamination is low, as indicated by $^{40}Ar/^{36}Ar$ ratios up to 948 (OLD-2 sample), which is among the highest values ever measured for volcanic gases. The $^{3}He/^{4}He$ ratio (6.9 Ra) is in the low range of MORB values, and neon has a MORB-like isotopic composition. Fischer et al (2009) interpreted the C, N and noble gas compositions as reflecting degassing of a new batch of magma from a MORB-like source. A $^{4}He/^{40}Ar^{*}$ ratio of 0.4 (*Table 2*) lower than the mantle range (1.8-3.0) is consistent with this interpretation because less soluble argon in silicate melts tends to degas more readily than more soluble helium during the first stages of magma degassing.

Gases extracted from two well-studied, gas-rich, basaltic glasses are also included in this compilation for the purposes of comparison. 2ΠD43 is a MORB glass from the Mid-Atlantic Ridge at 14°N (Javoy and Pineau, 1991; Moreira et al., 1998). This sample is considered to best represent the composition of a MORB gas phase. DICE corresponds to a subglacial glass sampled in Iceland (N64°10'31.9"/W021°02'43.0") which is also a reference sample that is considered representative of unfractionated mantle plume-sourced gas (Harrison et al., 1999;

Mukhopadhyay, 2012). Both samples have $^{4}He/^{40}Ar^{*}$ close to, or within the range of accumulation/production mantle values, indicating limited, if any, degassing fractionation.

3. Data handling

In order to determine the mantle source compositions, gas data need to be corrected for atmospheric contribution and fractional degassing of magmas, respectively, which we explain below.

3.1- Correction for atmospheric contamination

The correction for atmospheric contamination is negligible for CO_2 given its low atmospheric concentration (440 ppmv) but can be important for N_2 and Ar which are abundant in air (78.08 vol % and 0.93 vol%, respectively; *Table 1*). Atmospheric contamination of natural gases is always critical for non-radiogenic noble gases (e.g., ^{36}Ar) and can overprint the original composition. This is less of a problem for ^{40}Ar because this isotope is more abundant in the mantle than primordial ^{36}Ar relative to the atmosphere ($^{40}Ar/^{36}Ar$ = 298.6 in air versus ≥ 10,000-40,000 in the mantle, see below). Correction for atmospheric contamination is achieved using measured $^{40}Ar/^{36}Ar$ ratios:

$$^{40}Ar_{ca} = \frac{^{40}Ar_{meas}}{1+\alpha} \quad (2)$$

with:

$$\alpha = \left(\frac{^{36}Ar}{^{40}Ar}\right)_{ca} = \frac{\left(\frac{^{36}Ar}{^{40}Ar}\right)_{meas} - \left(\frac{^{36}Ar}{^{40}Ar}\right)_{atm}}{\left(\frac{^{36}Ar}{^{40}Ar}\right)_{atm} - \left(\frac{^{36}Ar}{^{40}Ar}\right)_{mantle}} \quad (3)$$

Where suffixes *ca*, *meas*, *atm* and *mantle* refer to $^{40}Ar/^{36}Ar$ values corrected for atmospheric contamination, measured in the sample, in the atmosphere and the mantle end-member, respectively. For the latter, we chose 40,000 and 10,000 for convective mantle and mantle plume sources, respectively (Bekaert et al., 2019; Mukhopadhyay, 2012). Taking 27,000 as the mantle source endmember of 2ΠD43 (Moreira et al., 2018) would have a minor effect on the correction. The corrections for the ^{40}Ar concentrations are in most cases marginal (within 0.1- 20 %), except for the Mud Volcano and Turbid Lake samples (65-71%) and for the Bublak gas sample (54%).

For N_2 which is also less affected by atmospheric contamination than primordial noble gases ($(N_2/^{36}Ar)$ = 1.5-3 x 10^4 in air and air-saturated water, and ≥10^6 in the mantle), the correction is achieved by using the $N_2/^{40}Ar$ ratio, with corrected N_2 being computed using the corrected $^{40}Ar_{CA}$ concentration:

$$\left(\frac{N_2}{^{40}Ar}\right)_{ca} = \left(\frac{N_2}{^{40}Ar}\right)_{meas} + \alpha \times \left[\left(\frac{N_2}{^{40}Ar}\right)_{meas} - \left(\frac{N_2}{^{40}Ar}\right)_{atm}\right] \quad (4)$$

$$N_{2,ca} = \left(\frac{N_2}{^{40}Ar}\right)_{ca} \times {}^{40}Ar_{ca} \quad (5)$$

where α is computed from *Eqn. 3*. The atmospheric contaminant for geothermal and volcanic gases is generally carried by underground aquifers (Giggenbach, 1980). For the atmospheric $(N_2/^{40}Ar)_{atm}$ ratio, we assume a value 39.2, which is a mean for air-saturated water at equilibrium temperatures of 10°C (37.9) and 100°C (40.5) (computed with the Bunsen coefficients given in Ozima and Podosek, 2002).

3.2- Correction for fractional degassing

As for oceanic basalts, the correction for fractional degassing is based on the measurement of the $^{4}He/^{40}Ar^{*}$ ratio using *Eqn. (1)*, where $^{40}Ar^{*}$ is approximated by $^{40}Ar_{ca}$. The abundance of helium does not need to be corrected for atmospheric contamination given its low atmospheric content (5.24 ppmv) and the generally low level of air contamination for the gases selected here (correction for the He isotopic ratios are also negligible for these samples). The $^{4}He/^{40}Ar^{*}$ ratios of the gases (including gases trapped in DICE and 2ΠD43 vesicles) range between 0.4 (Oldoinyo Lengai) and 2.3 (DICE) (*Table 2*). These values are much closer to the mantle production/accumulation range (1.8-3.0) than ratios measured in oceanic basalt glasses (3-96; Marty and Zimmermann, 1999), making correction for fractional degassing limited. Contrary to MORB glasses which are extensively degassed, CO_2-rich gases represent a gas phase in equilibrium with a degassing batch of magma and may also be related to new batches of rising magmas as in the case of Oldoinyo Lengai (Fischer et al., 2009) and Etna (Caracausi et al., 2003). The *C/N*, $C/^{3}He$, $N/^{3}He$ and $^{36}Ar/N$ ratios corrected for atmospheric contamination and fractional degassing are given in *Table 2* and *Table 3*, respectively.

4- Discussion

4.1- Distribution of C/N values in CO_2-rich gases and MORBs

In *Fig. 1* we compare the distribution of corrected *C/N* ratios in CO_2-rich gases and in the two gas-rich glasses (2ΠD43 and DICE) with that of all corrected MORB data (Marty and Zimmermann, 1999). The distribution of CO_2-rich gas data shows a mean *C/N* around 500 whereas the distribution of MORB values is shifted towards low N-MORB values, which

were more numerous than carbon-rich E-MORB values in the compilation of Marty and Zimmermann (1999). Hence data from natural gases confirm that the respective magma sources have *C/N* ratios higher than Solar, Chondritic (CI and CM, Fig. 5) and the mantle value previously proposed by Bergin et al (2015).

4.2- Crustal or subcontinental lithospheric mantle (SCLM) contribution?

Although gas compositions reported here indicate that *C/N* and $C/^3He$ ratios are comparable to those of the mantle sources of oceanic basalts (*Figs. 1 & 2*; *Tables 2 & 3*), the underlying crust and/or subcontinental lithospheric mantle may also significantly contribute to the budget of outgassing volatiles. We note that the isotopic compositions of carbon and nitrogen are consistent with a mantle origin ($\delta^{13}C$ =-5±2‰; $\delta^{15}N$=-5±2‰ for MORBs and diamonds, $\delta^{15}N$=0±3‰ for mantle plumes; e.g., Javoy and Pineau, 1991; Marty and Zimmermann, 1998; Marty and Dauphas, 2003; Cartigny et al, 2014) for these gases (*Table 1*), although some of the values are intermediate between those of carbonates ($\delta^{13}C$ =0) and of the atmosphere ($\delta^{15}N$=0‰), respectively, suggesting contributions of surface and/or crustal volatiles. The $^3He/^4He$ ratios of some of the CO_2-rich gases considered here (3.2 Ra for New Mexico gases, 4.4-5.9 Ra for continental Europe gases, 2.4 Ra for Yellowstone gases sampled outside the caldera) are lower than the canonical MORB range of 8±1 Ra, and samples from inside the Yellowstone caldera. This is also consistent with contributions of radiogenic ^{4}He from the regional crust.

Here we investigate crustal C (and by extension N) contribution to mantle-derived gases by using the $C/^3He$ ratios, which constitute a good indicator of C provenance since the crust is highly depleted in primordial ^{3}He relative to the mantle. In a $C/^3He$ versus *C/N* diagram (*Fig.*

312 *2*), several of the samples plot close to the field defined by MORBs and are intermediate
313 between the mean N-MORB and the carbon-rich E-MORB endmembers. However, some of
314 the data points also seem to depart from the mixing trend between these two MORB
315 endmembers. This tendency is best exemplified by the Eger Rift sample (*Fig. 2a*), but it could
316 also be the case for the New Mexico and Eifel samples. For the Eifel samples, Labidi et al
317 (2020) argued from N isotope systematics that crustal contamination of the gas is unlikely.
318 However, these authors did not exclude the contribution of ancient subducted crust to the
319 subcontinental mantle in Western Europe. For the Yellowstone gases, Werner and Brantley
320 (2003) estimated that ~50% of CO_2 is of sedimentary origin for the emanations outside the
321 caldera and that more than ~70% CO_2 is magmatic inside the caldera. In line with this view,
322 we note that the $CO_2/^3He$ ratios at Mud Volcano in the center of the caldera are lower (2.5 x
323 10^9) than those of the Brimstone basin gases (4 x 10^9) located outside the caldera, despite
324 having comparable $\delta^{13}C$ values (*Table 1*). Labidi et al (2020) concluded from N isotopologues
325 that the contribution of crustal nitrogen to the Yellowstone gases inside the caldera is
326 negligible. Overall the $C/^3He$ ratio of the Yellowstone gases inside the caldera (2.7 x 10^9) is
327 comparable to the Icelandic DICE ratio (2.8 x 10^9) (*Table 3*), where crustal contamination is
328 minimal.
329
330 In principle it should be possible to correct C for crustal contribution using *the* $CO_2/^3He$ ratios,
331 but this is complicated by the fact that E-type MORB glasses or plume samples also have
332 elevated $CO_2/^3He$ ratios (up to 6 x 10^9) and high $CO_2/^3He$ ratios could be due to mantle source
333 heterogeneities and not crustal contamination of magmas or related gases. In a $C/^3He$ versus
334 *C/N* diagram plot (*Fig. 2b*), contributions of pure crustal C (without crustal N) will produce
335 correlations anchored at the mantle end-member values and extending toward high $C/^3He$ and
336 *C/N* ratios. Each data point is corrected for crustal C contribution by extrapolating measured

337 data towards zero and taking the intersection of these lines with the $CO_2/^3He$ ratio inferred for
338 the mantle (2.2±0.6 x 10^9, Marty and Zimmermann, 1999 or 1.7±0.2 x 10^9, Tucker et al.,
339 2018; *Fig. 2b*). With these two $CO_2/^3He$ values, the mantle source *C/N* ratios are constrained
340 to be within 100-530 (*Fig. 2b*).
341
342 There is however two caveats with this approach. Firstly, the dispersion of data can be
343 accounted for by preferential loss of ^{3}He while leaving unaffected C and N (near-constant
344 C/N ratio), as suggested by one reviewer. In this case, the observed C/N ratios should be
345 representative of the mantle source value(s). Secondly, the correction for crustal C addition
346 assumes that only C, and not N, is contributed by the crust. To check this assumption, the
347 $C/^3He$ ratios are plotted as a function of the $N/^3He$ ratios in Figure 3 (data from *Table 2*). Data
348 seem to define two domains that both originate from the N-MORB composition, one
349 encompassing the E-MORB endmember and the other one pointing toward high $N/^3He$ values
350 and encompasses most of continental gas data. This correlation corresponds to a *C/N* ratio
351 around 400-500 (*Fig. 3*). However, a typical crustal *C/N* ratio would be ≤ 70 (with C = 27±5
352 ppmw, Hirschmann, 2018, and N = 0.50±0.04 ppmw, Johnson and Goldblatt, 2015) and
353 cannot therefore account for the elevated *C/N* ratio of the CO_2-rich gases.
354
355 The sub-continental lithospheric mantle (*C/N* = 390±260, computed with C = 100±20 ppmw,
356 Hirschmann, 2018, and N = 0.3±0.2 ppmw, Johnson and Goldblatt, 2015) could be a possible
357 endmember for some of the continental gases (*Fig. 3*), but other geochemical and geophysical
358 evidence support an asthenospheric, rather than lithospheric, origin for Cenozoic magmatism
359 in these regions. Evidence include: (i) trace element and isotope systematics of erupted lavas
360 (Hoernle et al., 1995); (ii) geochemical affinities with HIMU-type magmatism for Eifel
361 (Bekaert et al, 2019, and refs. therein, Sicily (Mt. Etna; Caracausi et al., 2003, and refs.

362 therein), Tanzania (Oldoinyo Lengai; Fischer et al., 2009, and refs. therein) and New Mexico
363 (Fitton et al., 1988), and (iii) geophysical imaging showing upwelling of asthenospheric
364 material below European magmatic provinces (Hoernle et al., 1995). Thus, the C-N-^{3}He
365 signatures of related CO_2-rich gases are likely to reflect the composition of asthenospheric
366 sources different from those feeding mid-ocean ridges. Enrichments in C and N compared to
367 typical MORBs (*Fig. 3*) may be due to primordial heterogeneities, or the recycling of surface
368 C and N deep into the mantle (Busigny and Bebout, 2013), in line with the HIMU character of
369 some of the corresponding magmatic provinces. In support of this possibility, Labidi et al.
370 (2020) argued from N isotopologues that about 30% of nitrogen in the Eifel CO_2-rich gases
371 could be recycled in origin.
372
373 Contribution of C-rich material into the mantle sources of E-MORBs and of intraplate
374 volcanoes could potentially account for the high *C/N* component suggested by trends
375 displayed in *Fig. 3*. It is not clear however if the high *C/N* ratio of the Icelandic DICE sample
376 and of the (inside caldera) Yellowstone samples have a similar recycled origin. Labidi et al.
377 (2020) proposed that nitrogen in Yellowstone gases defines a primordial mantle plume
378 signature having a $\delta^{15}N$ value close to 0‰ (+3±2 ‰) and a $N/^{36}Ar$ ratio of 2.4-3.9 x 10^6.
379 Marty and Dauphas (2003) also noted that plume-related gases have $\delta^{15}N$ values close to 0‰
380 (-1.5 to 3.3 ‰ for DICE) but these signatures were instead attributed to recycling of surface N
381 into the source of mantle plumes (Marty and Dauphas, 2003; Halldorson et al, 2016). We note
382 that the *C/N* ratios are different between Yellowstone (400-500) and Icelandic (1200-1400)
383 samples (*Table 2*), suggesting that the *C/N* ratio of the deep mantle is heterogeneous as a
384 possible result of different mixings between primordial and recycled nitrogen.
385
386 *4.3- The C/N ratio of the mantle*

We attempted to estimate the *C/N* ratio of the BSE using a mass balance involving nitrogen and mantle *C/N* ratios (Supplementary Material). As in previous work, this approach is based on (i) the bulk K content of the BSE (Arevalo et al, 2009) and K-Ar-N systematics of MORB and OIB-related samples (Marty, 1995; Marty and Dauphas, 2003; Johnson and Goldblatt, 2015; Bergin et al, 2015; Hirschmann, 2018), which are used to estimate the BSE N content, and (ii) the C/N ratios measured in MORB and OIB basalt glasses (Marty, 1995; Marty and Dauphas, 2003) and in mantle-derived CO_2-rich gases (this study). In doing so, we assume that the C/N ratios measured in surface basalts are representative of the mantle source composition, after correction for fractional degassing and atmospheric contamination (see Introduction). Because we selected samples from both the convective mantle (MORB glasses, CO_2-rich gases with MORB-like noble gas composition, e.g., Ne isotopes) and from OIB-like mantle domains including high-$^3He/^4He$ plumes (Iceland, Yellowstone), we further posit that these samples are representative of not only the convective mantle responsible for feeding mid-ocean ridges, but also encompass mantle plume domains. However, this approach relies on the assumption that the C/N ratio measured in mantle-derived basalts and gases is representative of the whole mantle composition from its shallowest regions down to the core-mantle interface, which is not guaranteed. There are some suggestions from diamond studies that the C/N ratio of mantle fluids from which diamonds formed may vary with depth, although such variations could result from processing during diamond formation rather than from compositional variation of the mantle itself (e.g., Mikhail andHowell, 2016, and refs. therein).

With these caveats in mind, we considered two data sets; the previously published MORB data (Marty and Zimmermann, 1999), and the volcanic/geothermal gas data presented in this

study. In order to estimate the mantle and BSE *C/N* ratios, we carried out Monte Carlo simulations following three approaches as detailed in Supplementary Material. We also estimated the $^{36}Ar/N$ ratios of the surface and mantle reservoirs in order to further constrain the composition of the BSE (*Table 4*).

Approach 1 uses gas data only (without gas-rich glasses) for the mantle. The corresponding samples tap large magmatic gas reservoirs which are more prone to homogenize the chemical compositions, and for which the effects of fractional degassing are limited. In this approach we use the mean *C/N* ratio of 541 and its standard deviation of 199 (computed with CO_2-rich gas data from *Table 2*; for each sample we took the average of the two numbers obtained with $^{4}He/^{40}Ar^*$ values of either 1.8 or 3.0).

Approach 2 also relies on the gas data only, using a median *C/N* value of 474, and an interquartile range ((IQR= 75th percentile - 25th percentile = Q3 - Q1 = 618-399 = 219). The fact that the mean and the median values are close is consistent with the observed near-Gaussian distribution of gas data (*Fig. 1* and *Fig. S1*).

Approach 3 considers all available data for MORB and gases. When taking this approach, the distribution becomes non-Gaussian and we therefore use median and IQR values.

In the following we considered only *Approaches 2 and* 3 (median and quartiles) given the non-Gaussian distribution of MORB *C/N* data that prohibits using means and standard deviations. For the sake of homogeneity, we also considered median and quartiles for the $^{36}Ar/N$ values of the mantle and of the BSE. The outcomes of these calculations are summarized in *Table 4* and displayed in *Fig. 4*. Our new range of best estimates for the

mantle *C/N* ratio is between 350-420, which is significantly higher than the ratio of ~90 obtained from the CO_2/Ba calibration (Bergin et al., 2015; Hirschmann, 2018), although marginally compatible when taking into account the large range of uncertainties (Q1: 167, G3: 618). We nevertheless assert that our estimate is representative of the mantle value(s) because low mantle *C/N* values predicted from the CO_2/Ba approach are rarely observed in MORBs or CO_2-rich gases. Doing so, we estimated a mantle C content around 330-450 ppmw (*Table 4*), which is higher than values previously suggested (e.g., 110±40 ppmw; Hirschmann, 2018), although the range of uncertainties is also large (Q1: 157, Q3: 583).

4.4- Origin of the BSE C/N ratio

From our newly computed mantle *C/N* ratio we estimated BSE *C/N* ratio to be 158-219 (range of IQs: 112 - 259; *Table 4*), higher than the previously proposed value of ~60 (Bergin et al., 2015), further emphasizing the non-canonical composition of terrestrial volatiles pointed out by Bergin et al. (2015). The high *C/N* ratio of the mantle could have resulted from preferential sequestration of nitrogen in planetary cores compared to carbon during Earth's formation events and/or during differentiation of parent planetesimals (Marty, 2012; Roskosz et al., 2013). However, experimental evidence does not support a higher metal-silicate partitioning of N compared to C (Dalou et al, 2017), although the role of other elements like H and pressure need to be assessed (Grewal et al, 2020). One possibility is that the metal-silicate partitioning behavior of C/N could be dependent on pressure, which remains to be experimentally constrained"

Preferential degassing of nitrogen during accretionary processes and its subsequent loss to space, possibly combined with metal-silicate partitioning, was proposed as an alternative (Bergin et al., 2015). It is not clear if magma degassing during Earth's accretionary events

462 could have fractionated enough N relative to C to account for the BSE C/N ratio, which
463 signature might have been inherited from planetary bodies that accreted to form the Earth
464 (Hirschmann, 2016). Alternatively, Liu et al. (2019) proposed the formation of nitrogen-rich
465 immiscible liquids that would have removed N from the forming mantle material during
466 metal-silicate interaction.
467
468 Here we add a supplementary dimension to this problem by adding the noble gas/nitrogen
469 ratios. In *Fig.* the *C/N* ratios of meteorites and terrestrial reservoirs are plotted against the
470 $^{36}Ar/N$ ratios (Supplementary Material). The different meteorite groups appear to define a
471 cosmochemical trend from CI-CM, EC and CR groups towards CV and CO groups (and
472 possibly ureilites) having elevated *C/N and* $^{36}Ar/N$ ratios. The CV (and CO) chondrites are
473 depleted in volatile elements (including C, N and noble gases) and moderately volatile
474 elements compared to CM-CIs (Palme and O'Neill, 2013). CVs, which are metamorphized to
475 variable extent, are depleted in volatile elements and thought to represent the non-
476 differentiated upper layers of a differentiated planetary body (Elkins-Tanton et al, 2011). The
477 silicate Earth also presents a monotonous depletion of moderately volatile elements
478 (compared to CI-CM chondrites) that, although more pronounced, resembles that of CVs
479 (Palme and O'Neill, 2013; Braukmüller et al, 2019). This trend cannot be due solely to
480 nebular condensation and is instead consistent with volatile loss during highly energetic
481 events (e.g., impacts) and/or from metamorphism on planetary parent bodies. Hence the
482 cosmochemical trend of meteorite families *(Fig. 4)* may represent the combined effects of
483 parent body metarmophism and partial differentiation. These processes resulted in (i) the
484 depletion of nitrogen relative to C and ^{36}Ar, and (ii) the moderately volatile element depletion
485 trend observed in evolved planetary bodies including the Earth.
486

Because Ar is not as depleted as N (*Fig. 4*), this differential behavior of these two elements may be due to variable retention rates of their respective host phases. Indeed, meteoritic noble gases are trapped in a refractory phase (the poorly-defined Q phase associated with insoluble organic matter - IOM) whereas a considerable fraction of nitrogen is trapped in less refractory organics like the soluble organic matter (SOM). Due to the much higher thermal sensitivity of the SOM relative to the IOM (Remusat 2015), the preferential loss of N over noble gases could be accounted for by a preferential destruction of labile, N-bearing organic phases relative to the more refractory, noble gas-bearing ones. An alternative possibility would be the formation of N-rich liquids and subsequent degassing/loss to space as proposed by Lui et al. (2019), which would have depleted N only, and not C nor Ar, from forming planetesimals or proto-Earth.

The fact that the C-N-Ar signature of the BSE is within the field of CV-CO data does not imply that the building blocks of Earth were made of this material. Conversely we propose that Earth was made of an assemblage of precursors that condensed and evaporated at various temperatures, which are best represented from a volatile element perspective by the CV chondrites. This possibility is independently supported with the monotonous volatile depletion trend of the silicate Earth that parallels that of CVs (Palme and O'Neill, 2013; Braukmüller et al, 2019).

4.5- *Terrestrial fractionation*

The terrestrial reservoirs (surface and mantle) clearly plot outside the meteoritic trend *(Fig. 5)*. The surface of Earth has a *C/N* ratio compatible with the range of CI-CMs but its $^{36}Ar/N$ ratio is in the range of CV-CO values, whereas the terrestrial mantle has an elevated *C/N* ratio akin

of CV-COs, but its ratio $^{36}Ar/N$ ratio is within the range of CI-CM-ECs. Hence none of these reservoirs can be directly linked to known chondritic compositions. However, summing up the *C, N* ^{36}Ar concentrations of these reservoirs, the obtained BSE composition falls on the cosmic trend and plots within the field of CV-COs, as explained in *Section 4.4*. We therefore propose that surface and the mantle compositions were established by chemical fractionation of the initial BSE, involving preferential incorporation, or retention, of C into the silicate Earth compared to volatile N and noble gases, and its corresponding depletion at the Earth's surface relative to N and noble gases.

The C/N ratio of the mantle, as estimated in this study (350-420), is in line with that outgassed at mid ocean ridges (385 ± 287), as calculated from the CO_2 (Marty and Tolstikhin, 1998) and N fluxes (5.7 ± 3.6 x 10^{12} mol/yr; Hirschmann, 2018 and references therein). The similarity between the mantle *C/N* estimated in this study and that degassed at MOR suggests that C and N are not significantly fractionated during degassing under the relatively oxidizing conditions that prevail in the present-day mantle (Hirschmann, 2016), as well as further supporting the validity of our mantle *C/N* estimates. Since both C and N are highly incompatible during mantle melting this is not unexpected but it does highlight that the long-term degassing from the mantle cannot account for the difference in *C/N* between the mantle and the surface. Therefore to explain the difference in the C/N between the mantle and the surface requires that C has been preferentially retained in the silicate Earth, or that volatile N has been preferentially lost of the Earth's surface.

Impacts during terrestrial accretion might have severely degassed impacting planetesimals, which themselves could have already been differentiated between a core, a silicate mantle and a proto-atmosphere and could therefore provide a mechanism for fractionation C and N. If N

was preferentially released to the early atmosphere, then during periods of impact driven atmospheric loss, nitrogen would be preferentially lost to space and the *C/N* of the Earth's surface would be lowered towards its present value. This mechanism has been previously suggested to account for the Earth's subchondritic *C/H* and *Cl/F* ratios (Tucker and Mukhopadhyay, 2014). For this mechanism to satisfactorily explain the low C/N of the Earth's surface requires that incompatibility of C and N during mantle melting was different than at present, with N being preferentially degassed relative to C. This may have been the case during the early Earth when the mantle was most likely dominated by reducing conditions (Aulbach and Stagno, 2016). However, recent experimental studies show that even under reducing conditions C and N may behave similarly with both likely being retained in the silicate mantle (Grewal et al., 2020). It therefore remains unclear whether N was preferentially degassed to, and subsequently lost from, the Earth's early atmosphere. Further constraints can also be gained by comparing the $^{36}Ar/N$ of the mantle and the Earth's surface reservoir (*Fig. 5*). Since Ar is a noble gas, it's solubility in mantle melts is not subject to differences in oxidation state and therefore even during reducing conditions, Ar would be concentrated in the atmosphere relative to the mantle. Episodes of atmospheric loss should therefore lower the $^{36}Ar/N$ in the atmosphere relative to the mantle, which is not the case. The role of atmospheric loss on the C/N of the surface reservoir therefore remains unclear and warrants further investigation.

The fractionation of C/N between the Earth's surface and the mantle may be the result of the long-term preferential recycling of C in the crust or the mantle. Li et al. (2019) proposed that the altered oceanic crust is the key carrier of C recycling into the mantle. An intermediate reservoir could be the arc crust (Barry et al. (2019) or the lithosphere (Kelemen and Manning, 2015), although this view has been challenged (Plank and Manning, 2019). These processes

might have been operative since the onset of plate tectonics but little is known about the tectonic regime of Early Earth. Recycling/sequestration of carbon should have been specific to this element with regard to nitrogen in order to yield the elevated C/N ratio of the mantle. Furthermore, recycling of C should have taken place early in Earth's history in order to avoid a Venus-like greenhouse effect. Sleep et al. (2001) proposed an elegant solution to this problem. These authors postulated that C might have been reintroduced into the mantle early in Earth's history through the foundering of crustal blocks that formed the lid of magma oceans (Hadean vertical tectonics). The carbonate formed in the crust would have formed directly from the massive CO_2 early atmosphere. If such a mechanism could transport C from the surface to the mantle, without venting CO_2 back to the atmosphere, then the fractionation of C and N between the mantle and the surface could have been an early feature. The early sequestration of C into the mantle is independently required to allow for clement temperature conditions and the formation of liquid water on the Earth's surface, which is known to have existed early on the Earth's surface. In order to achieve this and avoid the development of a CO_2 dominated atmospheres such as that that exists on Venus, large amounts of CO_2 must have been transported from the surface to the mantle and sequestrated there over geological timescales. To account for the different C-N-^{36}Ar compositions of the surface and the mantle, ~ 90 % of surface C should have been being sequestrated into silicates during these early episodes. Following the onset of plate tectonics subduction could have further augmented C sequestration in the mantle by preferential recycling C relative to N (Busigny and Bebout, 2013) and noble gases (Parai and Mukhopadhyay, 2019, and refs. therein). Carbon sequestration in the deep mantle either via early crustal foundering or subduction therefore not only plays a significant role in fractionating the C and N between the Earth's surface and interior but may play an essential role in modulating the Earth's climate and developing the conditions right for the emergence of life on the early Earth. The fact that the isotopic

587 composition of mantle carbon is comparable with that of surface carbon (Mackenzie and
588 Lerman, 2006) suggests that carbon sequestration did not fractionate its isotopes. In contrast,
589 N and noble gases were less efficiently homogenized between the surface and the mantle,
590 which permitted the survival of isotopic heterogeneities for these elements.
591
592 **5- Conclusions**
593
594 All sample considered in this study show high *C/N* and $^{36}Ar/N$ ratios relative to the surface
595 (atmosphere plus crust) inventory, pointing towards a mantle that has a unique volatile
596 composition when compared to cosmochemical reservoirs *(Fig. 5)*. The BSE composition
597 resembles that of chondritic groups (CV-CO) which are volatile-depleted and appear to have
598 experienced variable extent of metamorphism and planetary differentiation. We propose that
599 Earth formed from a range of already evolved planetary precursors that were depleted in
600 volatile and moderately volatile elements chemically (but not isotopically affected) akin to
601 CV and CO groups. Hence the high *C/N* character of the BSE may be inherited rather than
602 uniquely due to Earth's forming processes. In this scenario, most C (~90%) was preferentially
603 sequestrated into the mantle relative to volatile elements like N and noble gases early in
604 Earth's history, permitting habitable environmental conditions to develop at the surface of our
605 planet.
606
607 **Acknowledgments**
608
609 M.A, D.V.B, M.W.B, D.J.B and B.M were supported by the European Research Council
610 (PHOTONIS project, grant agreement No. 695618 to B.M.). Samples were collected as part
611 of Study # YELL-08056 - Xenon anomalies in the Yellowstone Hotspot. We would like to

612 thank Annie Carlson and all of the rangers at the Yellowstone National Park for providing
613 invaluable advice and help when collecting the samples. This work was partially supported by
614 a grant (G-2016-7206) from the Alfred P. Sloan Foundation and the Deep Carbon
615 Observatory to P.H.B as well as NSF award 2015789 to P.H.B. . Sampling at Mt. Etna and
616 gas analysis was supported by Instituto Nazionale di Geofisica e Vulcanologia Palermo.
617 Fruitful discussions with Marc Hirschmann helped us to shape the ideas presented in this
618 work. We acknowledge detailed and insightful reviews by Sami Mikhail and an anonymous
619 reviewer, and efficient editing by Frederic Moynier. This is CRPG contribution 2741.
620

621 **References**

622 1. Alexander, C.M.O., Bowden, R., Fogel, M.L., Howard, K.T., Herd, C.D.K., Nittler,
623 L.R., 2012. The provenances of asteroids, and their contributions to the volatile
624 inventories of the terrestrial planets. Science 337, 721–3.
625 doi:10.1126/science.1223474
626 2. Allègre, C.J., Hofmann, A.W., O'Nions, R.K., 1996. The argon constraints on mantle
627 structure. Geophys. Res. Lett. 23, 3555–3557.
628 3. Arevalo, R., McDonough, W.F., Luong, M., 2009. The K/U ratio of the silicate Earth:
629 Insights into mantle composition, structure and thermal evolution. Earth Planet. Sci.
630 Lett. 278, 361–369. doi:10.1016/j.epsl.2008.12.023
631 4. Aulbach, S. & Stagno, V., 2016. Evidence for a reducing Archean ambient mantle and
632 its effects on the carbon cycle. Geology 44, 751–754.
633 5. Ballentine, C.J., Holland, G., 2008. What CO_2 well gases tell us about the origin of
634 noble gases in the mantle and their relationship to the atmosphere. Philos. Trans. R.
635 Soc. A Math. Phys. Eng. Sci. 366, 4183–4203. doi:10.1098/rsta.2008.0150
636 6. Barry, P.H., Hilton, D.R., Füri, E., Halldorson, S.A., Grönvold, R. 2014. Carbon
637 isotope and abundance systematics of Icelandic geothermal gases and subaerial basalts
638 with implications for mantle-plume related CO_2 fluxes. Geochim. Cosmochim. Acta
639 134, 74-99, doi.org/10.1016/j.gca.2014.02.038
640 7. Barry, P. H., de Moor, J. M., Giovannelli, D., Schrenk, M., Hummer, D. R., et al.,
641 2019. Forearc carbon sink reduces long-term volatile recycling into the mantle. Nature
642 *568*, 487-492
643 8. Bekaert, D. V., Broadley, M.W., Caracausi, A., Marty, B., 2019. Novel insights into
644 the degassing history of Earth's mantle from high precision noble gas analysis of
645 magmatic gas. Earth Planet. Sci. Lett. 525, 115766. doi:10.1016/j.epsl.2019.115766

9. Bekaert, D. V, Broadley, M.W., Marty, B., 2020. The origin and fate of volatile elements on Earth revisited in light of noble gas data obtained from comet 67P / Churyumov- Gerasimenko Sci. Rep. 10:5796. doi:10.1038/s41598-020-62650-3
10. Bergin, E.A., Blake, G.A., Ciesla, F., Hirschmann, M.M., Li, J., 2015. Tracing the ingredients for a habitable earth from interstellar space through planet formation. Proc. Natl. Acad. Sci.. U.S.A. 112, 8965–8970. doi:10.1073/pnas.1500954112
11. Bräuer, K., Kämpf, H., Niedermann, S., Strauch, G., 2013. Indications for the existence of different magmatic reservoirs beneath the Eifel area (Germany): A multi-isotope (C, N, He, Ne, Ar) approach. Chem. Geol. 356, 193–208. doi:10.1016/j.chemgeo.2013.08.013
12. Bräuer, K., Kämpf, H., Niedermann, S., Strauch, G., Weise, S.M., 2004. Evidence for a nitrogen flux directly derived from the European subcontinental mantle in the Western Eger Rift, Central Europe. Geochim. Cosmochim. Acta 68, 4935–4947. doi:10.1016/j.gca.2004.05.032.
13. Braukmüller, N., Wombacher, F., Funk, C., Münker, C., 2019. Earth's volatile element depletion pattern inherited from a carbonaceous chondrite-like source. Nat. Geosci. 12, 564–568. doi:10.1038/s41561-019-0375-x
14. Broadley, M.K., Barry, P.H., Bekaert, D.V., Byrne, D.J., Caracausi, A., Ballentine, C.J., Marty, B., 2020. Identification of chondritic Proc. Natl. Acad. Sci. U.S.A. doi/10.1073/pnas.2003907117
15. Busigny, V., Bebout, G.E., 2013. Nitrogen in the Silicate Earth: Speciation and Isotopic Behavior during Mineral-Fluid Interactions. Elements 9, 353–358. doi:10.2113/gselements.9.5.353
16. Caracausi, A., Favara, R., Giammanco, S., Italiano, F., Paonita, A., Pecoraino, G., Rizzo, A., Nuccio, P.M., 2003. Mount Etna: Geochemical signals of magma ascent

671 and unusually extensive plumbing system. Geophys. Res. Lett. 30, 1057.
672 doi:10.1029/2002gl015463
673 17. Craig, H., Lupton, J.E., Welhan, J.A., Poreda, R., 1978. Helium isotopes ratios in
674 Yellowstone and Lassen volcanic gases. Geophis. Res. Lett. 5, 897–900.
675 18. Dalou, C., Hirschmann, M.M., von der Handt, A., Mosenfelder, J., Armstrong, L.S.,
676 2017. Nitrogen and carbon fractionation during core–mantle differentiation at shallow
677 depth. Earth Planet. Sci. Lett. 458, 141–151. doi:10.1016/j.epsl.2016.10.026
678 19. Dixon, J.E., Stolper, E.M., Holloway, J.R., 1995. An experimental study of water and
679 carbon dioxide solubilities in Mid-Ocean Ridge basaltic liquids. Part I: Calibration and
680 solubility models. J. Pet. 36, 1607–1631.
681 20. Elkins-Tanton, L.T., Weiss, B.P., Zuber, M.T., 2011. Chondrites as samples of
682 differentiated planetesimals. Earth Planet. Sci. Lett. 305, 1–10.
683 doi:10.1016/j.epsl.2011.03.010E
684 21. Fischer, T P, Burnard, P., Marty, B., Hilton, D.R., Furi, E., Palhol, F., Sharp, Z.D.,
685 Mangasini, F., 2009. Upper-mantle volatile chemistry at Oldoinyo Lengai volcano and
686 the origin of carbonatites. Nature 459, 77–80. doi:10.1038/nature07977
687 22. Fitton, J.G., James, D., Kempton, P.D., Ormerod, D.S., Leeman, W.P., 1988. The Role
688 of Lithospheric Mantle in the Generation of Late Cenozoic Basic Magmas in the
689 Western United States. J. Petrol. Special Lithospheric Issue, 331–349.
690 doi:10.1093/petrology/Special_Volume.1.331
691 23. Giggenbach, W.F., 1980. Geothermal gas equilibria. Geochim. Cosmochim. Acta 44,
692 2021–2032.
693 24. Goldblatt, C., Claire, M.W., Lenton, T.M., Matthews, A.J., Watson, A.J., Zahnle, K.J.,
694 2009. Early Earth. Nat. Geosci. 2, 1–6. doi:10.1038/ngeo692
695 25. Grewal, D.S., Dasgupta, R. and Farnell, A., 2020. The speciation of carbon, nitrogen,

and water in magma oceans and its effect on volatile partitioning between major reservoirs of the Solar System rocky bodies. Geochim. Cosmochim. Acta 280, 281-301.

26. Halldórsson, S.A., Hilton, D.R., Barry, P.H., Füri, E., Grönvold, K., 2016. Recycling of crustal material by the Iceland mantle plume: New evidence from nitrogen elemental and isotope systematics of subglacial basalts. Geochim. Cosmochim. Acta 176, 206–226. doi:10.1016/j.gca.2015.12.02
27. Hirschmann, M.M., 2016. Constraints on the early delivery and fractionation of Earth's major volatiles from C/H, C/N, and C/S ratios. *American Mineralogist* 101, 540–553.
28. Hirschmann, M.M., 2018. Comparative deep Earth volatile cycles: The case for C recycling from exosphere/mantle fractionation of major (H_2O, C, N) volatiles and from H_2O/Ce, CO_2/Ba, and CO_2/Nb exosphere ratios. Earth Planet. Sci. Lett. 502, 262–273. doi:10.1016/j.epsl.2018.08.023
29. Hoernle, K., Zhang, Y.-S., Graham, D., 1995. Seismic and geochemical evidence for large-scale mantle upwelling beneath the eastern Atlantic and western and central Europe. Nature 374, 34–39. doi:10.1038/374034a0
30. Jambon, A., Weber, H., Begemann, F., 1985. Helium and argon from an Atlantic MORB glass : concentration, distribution and isotopic composition. Earth Planet. Sci. Lett. 73, 255–268.
31. Javoy, M., Pineau, F., 1991. The volatiles record of a "popping" rock from the Mid-Atlantic Ridge at 14°N: chemical and isotopic composition of gas trapped in the vesicles. Earth Planet. Sci. Lett. 107, 598–611. doi:10.1016/0012-821X(91)90104-P
32. Johnson, B., Goldblatt, C., 2015. The nitrogen budget of Earth. Earth-Science Rev. 148, 150–173. doi:10.1016/j.earscirev.2015.05.006

721 33. Labidi, J., Barry, P.H., Bekaert, D. V., Broadley, M.W., Marty, B., Giunta, T., Warr,
722 O., Sherwood Lollar, B., Fischer, T.P., Avice, G., Caracausi, A., Ballentine, C.J.,
723 Halldórsson, S.A., Stefánsson, A., Kurz, M.D., Kohl, I.E., Young, E.D., 2020.
724 Hydrothermal $^{15}N^{15}N$ abundances constrain the origins of mantle nitrogen. Nature 580,
725 367–371. doi:10.1038/s41586-020-2173-4
726 34. Le Voyer, M., Hauri, E.H., Cottrell, E., Kelley, K.A., Salters, V.J.M., Langmuir, C.H.,
727 Hilton, D.R., Barry, P.H., Füri, E., 2019. Carbon fluxes and primary magma CO_2
728 contents along the global mid-ocean ridge system. Geochem., Geophys. Geosyst. 20,
729 1387–1424. doi:10.1029/2018GC007630
730 35. Li, K., Li, L., Pearson, D. G., & Stachel, T., 2019. Diamond isotope compositions
731 indicate altered igneous oceanic crust dominates deep carbon recycling. Earth Planet.
732 Sci. Lett., 516, 190-201.
733 36. Li, J., Chen, B., Mookherjee, M., Morard, G., 2020. Carbon versus other light
734 elements in earth's core, in: Deep Carbon. pp. 40–65.
735 37. Libourel, G., Marty, B., Humbert, F., 2003. Nitrogen solubility in basaltic melt. Part I.
736 Effect of oxygen fugacity. Geochim. Cosmochim. Acta 67, 4123–4135.
737 38. Liu, J., Dorfman, S.M., Lv, M., Li, J., Zhu, F., Kono, Y., 2019. Loss of immiscible
738 nitrogen from metallic melt explains Earth's missing nitrogen. *Geochem. Persp. Lett.*
739 11, 18–22.
740 39. Kelemen, P. B., & Manning, C. E., 2015. Reevaluating carbon fluxes in subduction
741 zones, what goes down, mostly comes up. Proceed. Nat. Acad . Sci., 112(30), E3997-
742 E4006.
743 40. Mackenzie, F.T. and Lerman, A., 2006. Carbon in the Geobiosphere: Earth's outer
744 shell. Springer, 341 pp. ISBN 978-1-4020-4238-6
745 41. Marty, B., 2012. The origins and concentrations of water, carbon, nitrogen and noble

gases on Earth. Earth Planet. Sci. Lett. 313–314, 56–66. doi:10.1016/j.epsl.2011.10.040

42. Marty, B., Dauphas, N., 2003. The nitrogen record of crust-mantle interaction and mantle convection from Archean to present. Earth Planet. Sci. Lett. 206, 397–410.

43. Marty, B., Tolstikhin, I.N., 1998. CO_2 fluxes from mid-ocean ridges, arcs and plumes. Chem. Geol. 145, 233–248.

44. Marty, B., Zimmermann, L., 1999. Volatiles (He, C, N, Ar) in mid-ocean ridge basalts: Assesment of shallow-level fractionation and characterization of source composition. Geochim. Cosmochim. Acta 63, 3619–3633.

45. Mikhail, S., Howell, D., 2016. A petrological assessment of diamond as a recorder of the mantle nitrogen cycle. Amer. Mineral. 101, 780–787.

46. Moreira, M., Kunz, J., Allègre, C.J., 1998. Rare gas systematics in Popping Rock : Isotopic and elemental compositions in the upper mantle. Science 279, 1178–1181.

47. Mukhopadhyay, S., 2012. Early differentiation and volatile accretion recorded in deep-mantle neon and xenon. Nature 486, 101–104. doi:10.1038/nature11141

48. Mukhopadhyay, S., Parai, R., 2019. Noble Gases: A Record of Earth's Evolution and Mantle Dynamics. Annu. Rev. Earth Planet. Sci. 47, 389–419. doi:10.1146/annurev-earth-053018-060238

49. Nakai, S., Wakita, H., Nuccio, M.P., Italiano, F., 1997. MORB-type neon in an enriched mantle beneath Etna, Sicily. Earth Planet. Sci. Lett. 153, 57–66. doi:10.1016/S0012-821X(97)00161-1

50. Ozima, M., Podosek, F.A., 2002. Noble gas geochemistry. Cambridge University Press, Cambridge.

51. Palme, H., O'Neill, H., 2013. Cosmochemical Estimates of Mantle Composition, 2nd ed, Treatise on Geochemistry: Second Edition. Elsevier Ltd. doi:10.1016/B978-0-08-

095975-7.00201-1

52. Plank, T. and Manning, C.E., 2019. Subducting carbon. Nature, 574, 343-352

53. Remusat, L. (2015). Organics in primitive meteorites. *EMU Notes in Mineralogy*, *15*, 1-33.

54. Rosenthal, A., Hauri, E.H., Hirschmann, M.M., 2015. Experimental determination of C , F , and H partitioning between mantle minerals and carbonated basalt , CO_2/Ba and CO_2/Nb systematics of partial melting, and the CO_2 contents of basaltic source regions. Earth Planet. Sci. Lett. 412, 77–87. doi:10.1016/j.epsl.2014.11.044

55. Roskosz, M., Bouhifd, M.A., Jephcoat, A.P., Marty, B., Mysen, B.O. (2013) Nitrogen solubility in molten metal and silicate at high pressure and temperature. *Geochimica et Cosmochimica Acta* 121, 15–28.

56. Sleep, N.H., Zahnle, K., Neuhoff, P.S., 2001. Initiation of clement surface conditions on the earliest Earth. Proc. Natl. Acad. Sci. U. S. A. 98, 3666–3672.

57. Staudacher, T., 1987. Upper mantle origin for Harding County well gases. Nature 325, 605–607.

58. Tucker, J.M. and Mukhopadhyay, S., 2014. Evidence for multiple magma ocean outgassing and atmospheric loss episodes from mantle noble gases. Earth Planet. Sci. Lett., 393, 254-265.

59. Tucker, J.M., Mukhopadhyay, S., Gonnermann, H.M., 2018. Reconstructing mantle carbon and noble gas contents from degassed mid-ocean ridge basalts. Earth Planet. Sci. Lett. 496, 108–119. doi:10.1016/j.epsl.2018.05.024

60. Werner, C., Brantley, S., 2003. CO_2 emissions from the Yellowstone volcanic system. Geochem., Geophys. Geosyst. 4. doi:10.1029/2002GC000473

61. Zartman, R.E., Wasserburg, G.J., Reynolds, J.H., 1961. Helium, argon and carbon in some natural gases. J. Geophys. Res. 66–1, 277–306.

Type	Country	Location	Sample name	Excess ^{129}Xe	Neon isotopes	CO_2 %	$\delta^{13}C$ ‰, PDB	N_2 %	$\delta^{15}N$ ‰, ATM	He ppmv	Ar ppmv	$^{3}He/^{4}He$, Ra	$^{40}Ar/^{36}Ar$	Refs.
CO2-rich gases														
CO2 well gas	USA	Bueyeros NM	Mitchell n°4	√	DMM	99.9	-3.9	0.12	n.d.	45	28	3.2	22500	1,2
CO2 well gas	USA	Bueyeros NM	Mitchell n°12	√	DMM	99.8	-4.1	0.15	n.d.	47	29	3.2	34000	1,2
Bubbling water	Germany	Eifel	Victoriaquelle	√	DMM	99.77	-2.1	0.18	-1.7	32	37	4.4	4040	3,4,5
Bubbling water	Germany	Eifel	Schwefelquelle	√	DMM	99.68	-2.0	0.24	-1.8	31	62	4.5	8287	3,4,5
CO2 well gas	Czech Rep.	Eger graben	Bublak	n.d.	n.d.	99.8	-2.0	0.20	-3.2	19	36	5.9	551	3
CO2 well gas	Italy	Etna area	Naftia	√	DMM	97.6	-1.0	0.53	n.d.	64	78	6.6	1445	6, 7
Volcanic gas	Tanzania	Oldoinyo Lengai	OLD-2	n.d.	DMM	99.34	-2.4	0.66	-4.1	27	90	6.9	947	8
Geothermal gas	USA	Yellowstone, inside	Mud Volcano 2A	n.d.	PM	98.50	-2.6	0.26	-8.6	15	40	14.4	414	5,7,9
Geothermal gas	USA	Yellowstone, inside	Mud Volcano 2B	n.d.	PM	98.10	-2.7	0.31	-1.9	18	77	13.8	450	5,7,9
Geothermal gas	USA	Yellowstone, border	Turbid Lake 3A	n.d.	PM	96.34	-2.9	0.23	-1.9	34	67	5.27	433	5,7,9
Geothermal gas	USA	Yellowstone, border	Turbid Lake 3B	n.d.	PM	96.55	-2.6	0.22	-0.1	38	62	5.19	433	5,7,9
Geothermal gas	USA	Yellowstone, outside	Brimstone Basin 4A	√	PM	98.15	-2.7	0.16	0.2	72	52	2.77	1536	5,7,9
Geothermal gas	USA	Yellowstone, outside	Brimstone Basin 4B	√.	n.d.	98.05	-2.8	0.16	-1.4	68	52	2.85	1417	5,7,9
Basaltic glasses														
MORB glass	Mid-Atlantic	14°N	2ΠD43	√	DMM	95.0	-3.7	0.12	-3.1	33	24	8.1	24500	10.11
Subglacial glass	Iceland	64°N	DICE	√	PM	99.9	-3.6	0.04	0.2	14	6.2	17.9	7047	12,13,14,15
Atmosphere						0.04		78.08	0	5.24	9340	1	298.6	16

Table 1: List of selected samples, chemical compositions and geodynamic settings. For the Yellowstone samples, *inside*, *border* and *outside* refer to the location of the sampled sites with respect to the limit of the caldera. DMM and PM refer to the depleted MORB mantle and the plume mantle, respectively, as defined by Ne isotopes measured in these samples. *The* $^{3}He/^{4}He$ ratios are expressed as multiples of the atmospheric value of Ra = 1.39 x 10^{-6}. "n.d": not determined. ppmv: part per million in volume. References: 1: Zartman et al. (1961); 2: Staudacher (1987); 3: Bräuer et al. (2013); 4: Bekaert et al. (2019); 5: Labidi et al. (2020) for N isotope data; 6: Nakai et al. (1997); for He, Ne and Xe isotope data; 7: Chemical analysis carried out at INGV Palermo. 8: Fischer et al. (2009); 9: Broadley et al (2020) for He, Ne and Xe isotope data; 10: Javoy and Pineau (1991); 11: Ne and He data from Moreira et al. (1998), the $^{40}Ar/^{36}Ar$ ratio is the highest value reported by these authors; 12: He, Ne and Xe isotope data from Mukhopadhyay (2012), the $^{40}Ar/^{36}Ar$ ratio is the highest value reported by this author; 13: Carbon isotopes for sample MD-1 from the same site (Barry et al., 2014); 14: Chemical analysis (CO_2, He isotopes) carried out at CRPG; 15: Marty and Dauphas (2003) for N isotopes; 16: Ozima and Podosek (2002).

Location	Name	Type	C/ N Meas.	N/ Ar Meas.	He/ Ar Meas.	N/ Ar Corr. Atm.	C/ N Corr. Atm.	^{4}He/ ^{40}Ar* Corr. Atm.	C/N Corr for atm. cont & degas. fract.	
									1.8	3.0
CO_2-rich gases										
Bueyeros NM	Mitchell n°4	DMM	416	86	1.59	86	417	1.60	459	688
Bueyeros NM	Mitchell n°12	DMM	333	103	1.60	103	333	1.60	366	549
Eifel	Victoriaquelle	DMM	277	97	0.87	101	285	0.94	479	718
Eifel	Schwefelquelle	DMM	208	77	0.50	79	211	0.52	565	847
Eger graben	Bublak	n.d.	249	100	0.53	108	559	1.15	798	1198
Etnean province	Naftia	DMM	92	136	0.82	161	98	1.03	152	228
Oldoinyo Lengai	OLD-2	DMM	76	145	0.30	192	83	0.43	256	384
Yellowstone, inside	Mud Volcano 2A	PM	189	130	0.39	355	241	1.35	304	456
Yellowstone, inside	Mud Volcano 2B	PM	158	81	0.23	158	232	0.67	511	767
Yellowstone, border	Turbid Lake 3A	PM	209	69	0.50	131	343	1.57	382	573
Yellowstone, border	Turbid Lake 3B	PM	219	71	0.61	139	352	1.92	334	502
Yellowstone, outside	Brimstone Basin 4A	PM	307	62	1.38	66	344	1.67	366	548
Yellowstone, outside	Brimstone Basin 4B	PM	306	62	1.31	67	348	1.61	379	569
Basalt glasses										
MAR 14°N	2ΠD43	DMM	396	100	1.36	101	396	1.37	492	738
Iceland 60°N	DICE	PM	1130	142	2.26	146	1141	2.26	952	1428

CO_2-rich gases, mean	**412**	**617**
All MORB	**535 ± 224**	
N-MORB	273 ± 106	
T-MORB	433 ± 392	
E-MORB	1839 ± 641	

Table 2: Abundance ratios of CO_2-rich gases (same notation as in *Table 1*). The ratios are corrected for atmospheric contamination using *Eqns. 2-5* (first three numerical columns). The 4th column gives the *C/N* ratio where the N content has been corrected for atmospheric contamination. The 5th column gives the $^{4}He/^{40}Ar^{*}$ ratio where ^{4}He equals to the He content and ^{40}Ar* is approximated by the total Ar content corrected for air contamination. n.d.: not determined. Note that the $^{4}He/^{40}Ar^{*}$ ratios are within, or close to, the mantle production/accumulation range of 1.8-3.0. The exact value of this ratio is not precisely known since it depends on the parent (K+U)/Th abundance ratio and on the residence time of noble gases in the respective mantle sources. The last two columns represent the *C/N* molar ratios corrected for atmospheric contamination and degassing fractionation. Correction for the latter has been made using *Eqn. 1* for the two end-member values of the mantle range. The mean *C/N* ratio of the CO_2-rich gases analyzed here excluding glass data (412-617) of with glass data (453-680) is consistent with the mean MORB (535±224; Marty and Zimmermann, 1999).

Location	Type	C/ ^{3}He	N/ ^{3}He	^{36}Ar/ N$^{\$}$	^{4}He/ ^{40}Ar*	C/^{3}He Corr. degas. fract. 10^{9}		N/^{3}He Corr. degas. fract. 10^{6}	
		Meas. 10^{9}	Corr. Atm 10^{6}	Corr. Atm 10^{-7}	Corr. Atm	1.8	3.0	1.8	3.0
CO2-rich gases									
Harding Bueyeros NM	CM	5.12	12.3	2.91	1.60	4.99	4.50	10.9	6.54
Harding Bueyeros NM	CM	4.88	14.7	2.43	1.60	4.76	4.29	13.0	7.81
Eifel	CM	5.01	18.1	2.46	0.94	4.38	3.94	9.15	5.49
Eifel	CM	5.06	24.3	3.18	0.52	3.91	3.52	6.93	4.16
Eger graben	n.d.	8.34	21.2	2.31	1.15	7.60	6.84	9.52	5.71
Etna area	CM	1.66	18.0	1.56	1.03	1.48	1.33	9.71	5.83
Oldoinyo Lengai	CM	3.82	50.3	1.30	0.43	2.85	2.56	11.1	6.67
Yellowstone	PM	3.29	17.4	2.82	1.35	3.10	2.79	10.2	6.12
Yellowstone	PM	2.86	18.1	6.32	0.67	2.33	2.09	4.55	2.73
Yellowstone	PM	1.42	6.8	7.61	1.57	1.38	1.24	3.62	2.17
Yellowstone	PM	1.26	5.7	7.21	1.92	1.28	1.15	3.82	2.29
Yellowstone	PM	3.87	12.6	15.1	1.67	3.80	3.42	10.4	6.25
Yellowstone	PM	4.39	14.3	15.0	1.61	4.29	3.86	11.3	6.78
Mean				5.40		3.55	3.20	8.79	5.27
Median				2.90		3.80	3.42	9.71	5.83
Basalt glasses									
MAR 14°N	CM	2.60	6.57	2.48	1.37	2.46	2.21	5.00	3.00
N 64°	PM	3.03	2.53	6.84	2.26	3.18	2.86	3.15	1.89

Table 3: *C/^{3}He*, *N/^{3}He* and *N/^{36}Ar* ratios of analyzed gases (same notation as in *Table 2*). $^{\$}$: *^{36}Ar/N* ratios corrected for atmospheric contamination assuming *^{40}Ar/^{36}Ar* ratios of 40,000 for the convective MORB mantle (Bekaert et al., 2019) and 10,000 for the plume mantle (Mukhopadhyay, 2012), respectively

	Surface	Mantle	BSE
N, ppmw	1.56±0.06	1.10±0.55	
C, ppmw	27±5	A2: $479\ ^{Q1:323}_{Q3:646}$ A3: $337\ ^{Q1:211}_{Q3:504}$	
^{36}Ar, 10^{-6} ppmw	50	$1.29\ ^{Q1:0.82}_{Q3:1.89}$	
C/N mol/mol	21±6	A2: $474\ ^{Q1:399}_{Q3:618}$ A3: $352\ ^{Q1:167}_{Q3:606}$	A2: $219\ ^{Q1:174}_{Q3:259}$ A3: $158\ ^{Q1:112}_{Q3:215}$
^{36}Ar/N, 10^{-7} mol/mol	124±5	$2.90\ ^{Q1:2.35}_{Q3:7.40}$	$74.3\ ^{Q1:65.7}_{Q3:85.2}$

Table 4: C, N and ^{36}Ar concentrations (inventories divided by the mass of the silicate Earth of 4 x 10^{27} g) and elemental ratios. For the surface of the Earth (atmosphere and crust), C and N data are from Hirschmann (2018) and refs. therein and the ^{36}Ar concentration corresponds to the atmospheric inventory (Ozima and Podosek, 2002), the crustal reservoir being neglected. For the mantle, the N concentration is from Hirschmann (2018) and the C and ^{36}Ar concentrations are computed from the mantle *C/N* and ^{36}*Ar/N* ratios estimated here (see text and Supplementary Material). A2 and A3 refer to *Approach 1* and *Approach 2*, respectively, as described in the main text and in the Supplementary Material section. A2 is median and interquartile range (between brackets, Q1 = 1st interquartile and Q3 = 3rd interquartile, respectively) of gas data only and A3 is median and interquartile range of gas+MORB data.

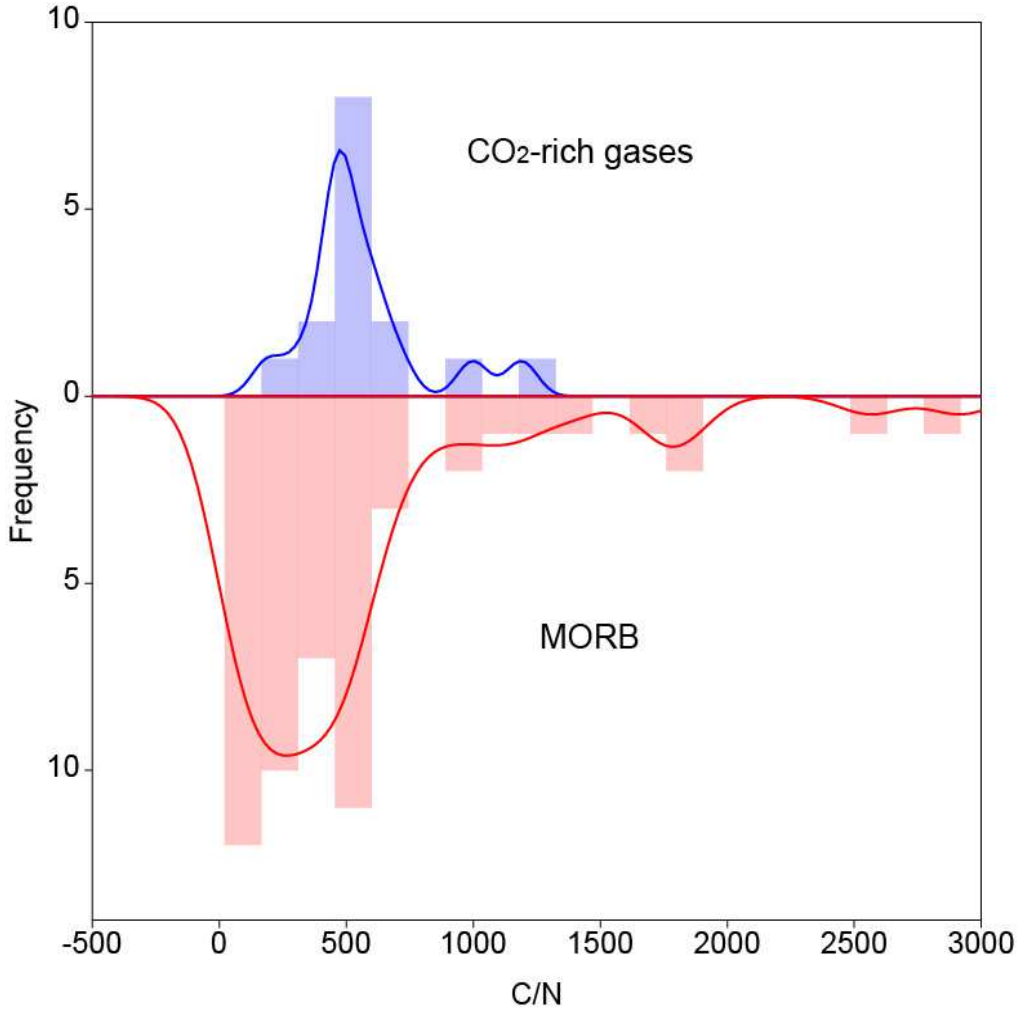

Figure 1: Kernel density distribution (made with Past4[@] software) of *C/N* ratios in CO_2-rich gases (this work, including gas-rich glasses) and MORB samples (Marty and Zimmermann, 1999). For the CO_2-rich gases, each data corresponds to the mean of the corrected ratios using $^{4}He/^{40}Ar^{*}$ of 1.8 or 3, assigning an uncertainty equal to the difference between the two calculated values (typically 20 %).

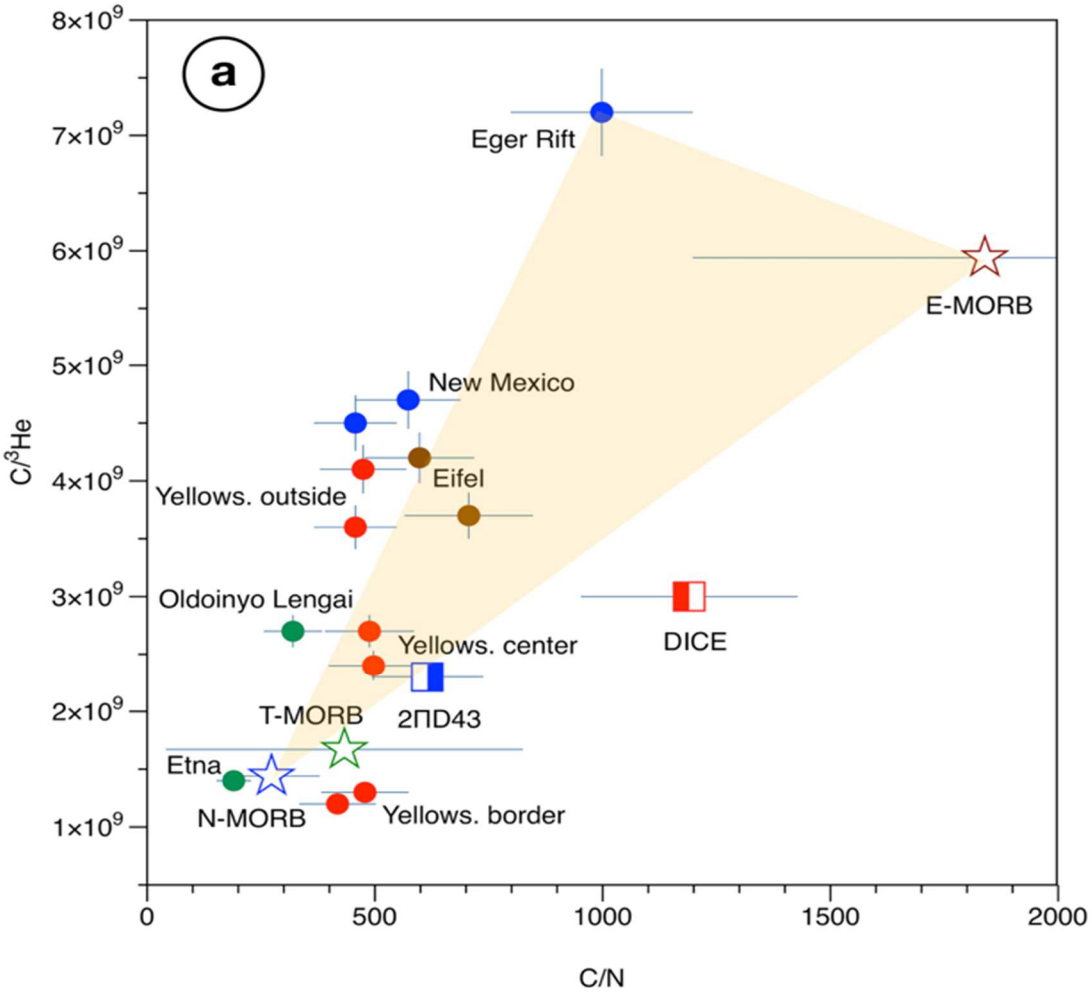

Figure 2a: *C/^{3}He* versus *C/N* for CO_2-rich gases (data from *Tables 2 & 3*). Red dots: Yellowstone gases; Green dots: volcanic gases; Brown dots: Eifel gases; Blue dots: New Mexico and Eger Rift gases. Variations can be understood as resulting from a 3-end-member mixing between N-MORB, E-MORB and a crust-influenced component (the latter exemplified by the Eger Rift Bublak gas.

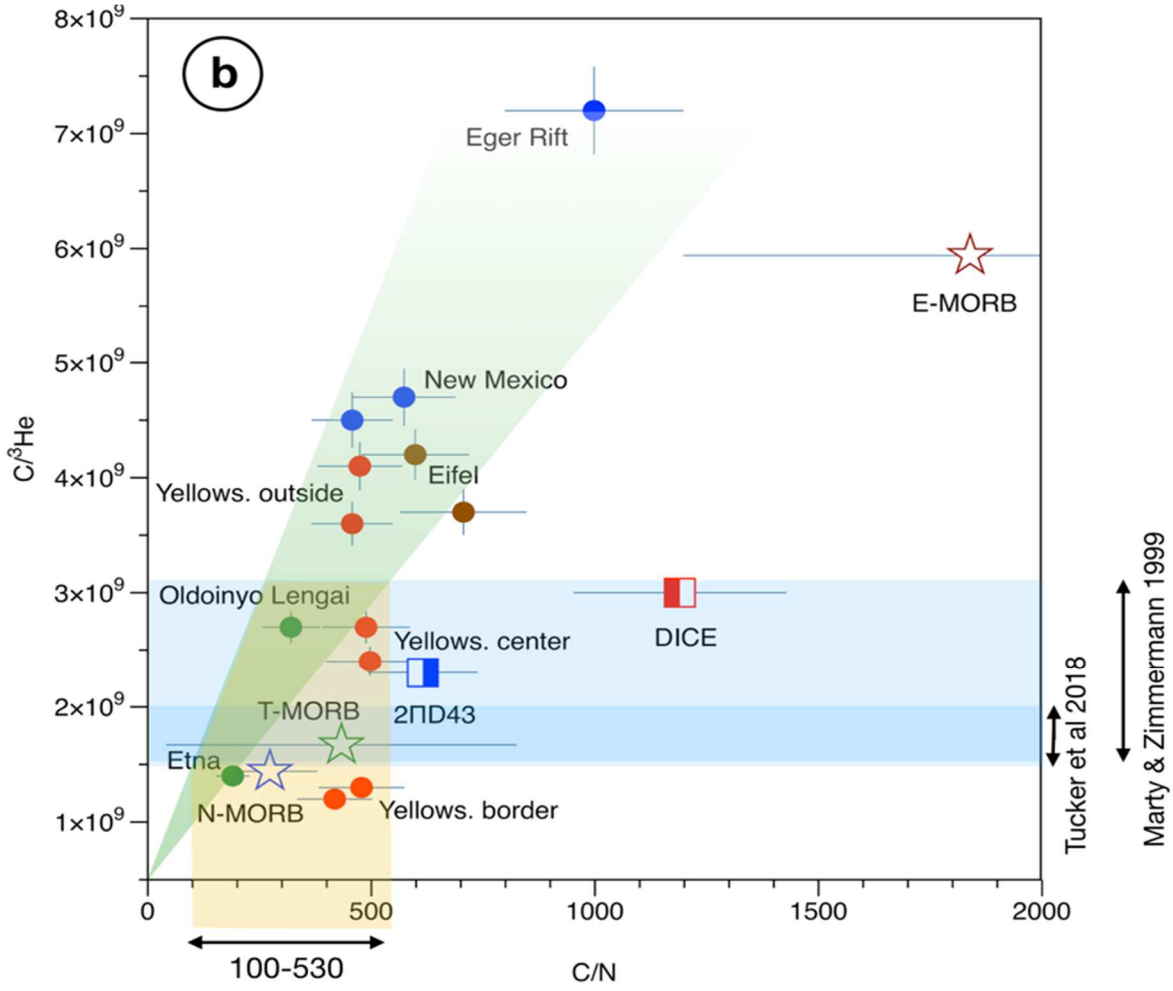

817

818

819

820

821

822 **Figure 2b:** same format as *Fig. 2a*. Attempt of correction for contribution of crustal C and N.

823 The green area represents $C/^3He$ and *C/N* ratios trending towards the origin (no carbon). N-

824 MORB and E-MORB averages are from Marty and Zimmermann (1999). The blue areas

825 represent the ranges of $C/^3He$ ratios for the MORB mantle according to Tucker et al. (2018)

826 and Marty and Zimmermann (1999), respectively. The mantle source *C/N* ratio is obtained by

827 intersecting the green area with the blue area.

828

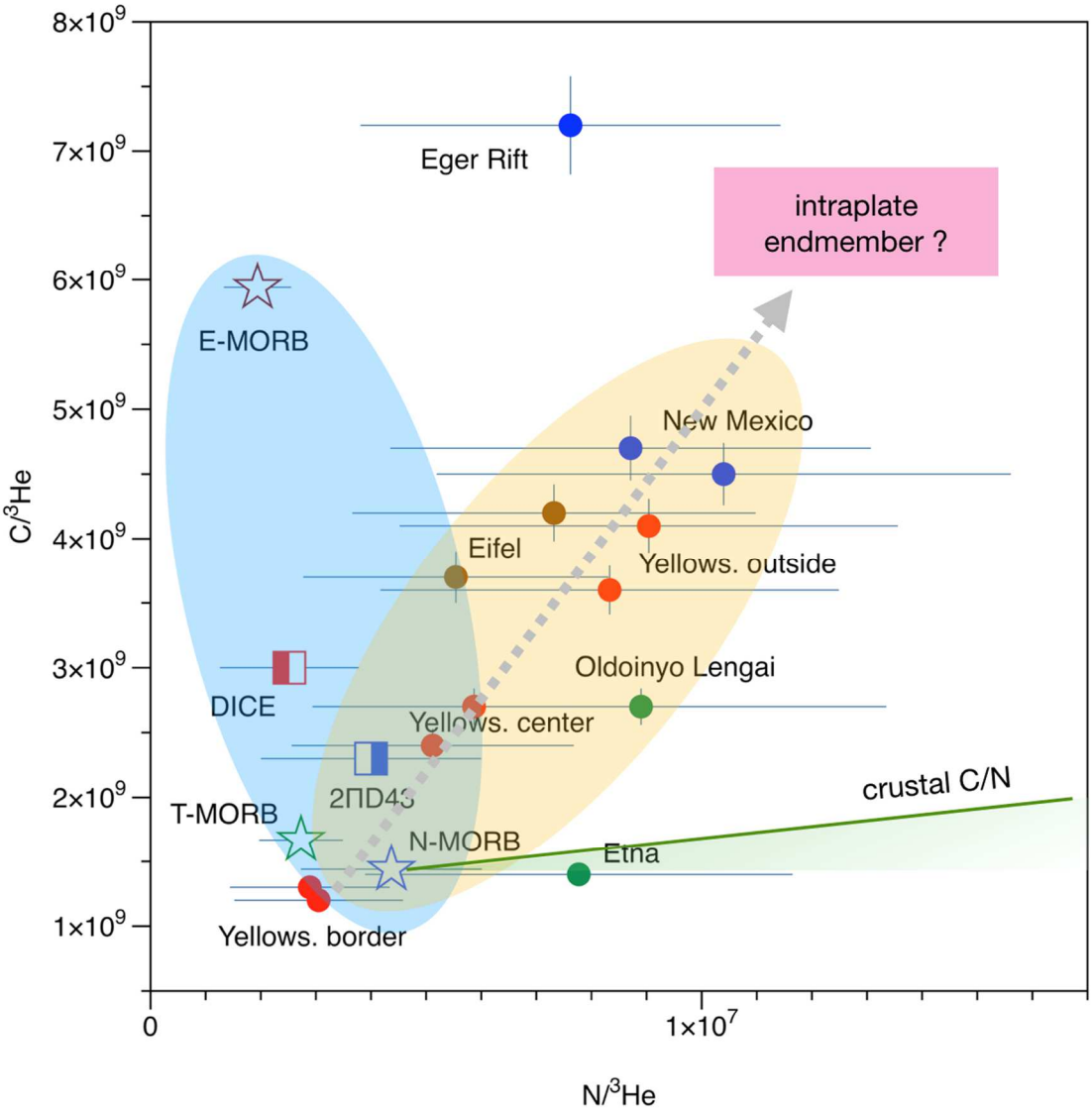

829

830

831 **Figure 3:** *C/³He* ratios as a function of the *N/³He* ratios for CO_2-rich gases. Same symbols as

832 in *Fig. 2*. The MORB ellipse (blue) encircles N-MORB and E-MORB values (Marty and

833 Zimmermann, 1999). The yellow ellipse encompasses CO_2-rich gases, with an approximate

834 slope corresponding to *a C/N* ratio of ~450, which is higher than the crustal ratio (≤ 70, see

835 *Section 4.2*). Uncertainties on the *N/³He* ratios are represented by the difference between

836 corrected values using the two possible mantle $^{4}He/^{40}Ar^{*}$ ratios (1.8 and 3.0).

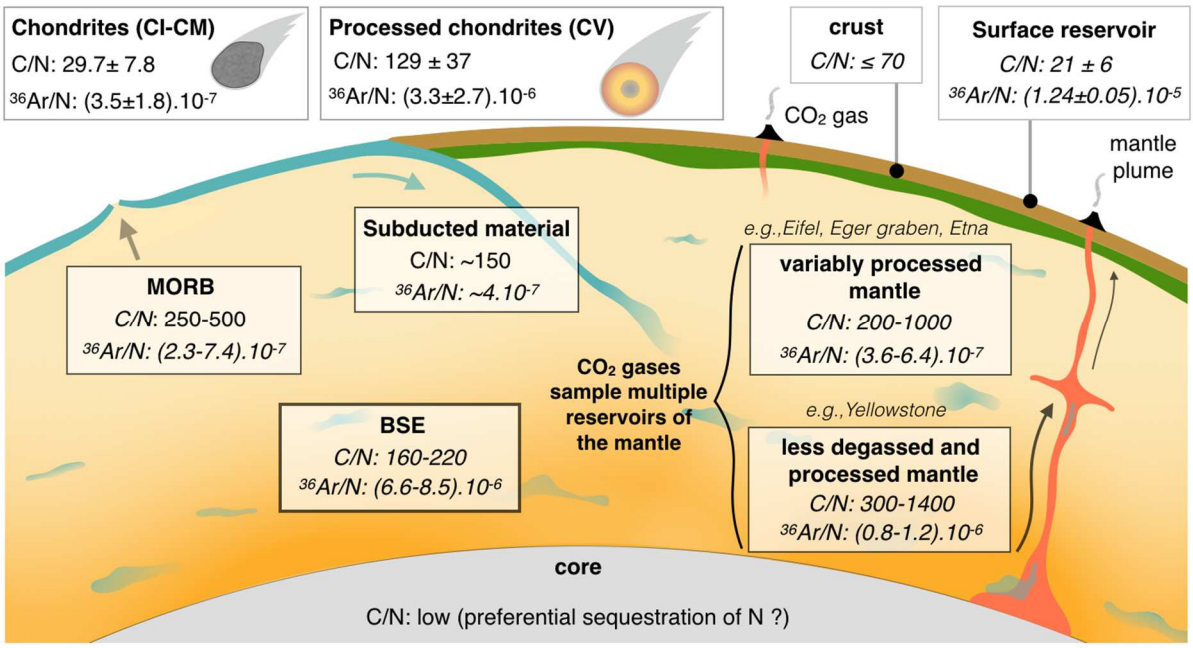

Figure 4: Graphic summary of the estimates presented in this work (data from *Tables 3 and 4*). Abundance ratios are molar.

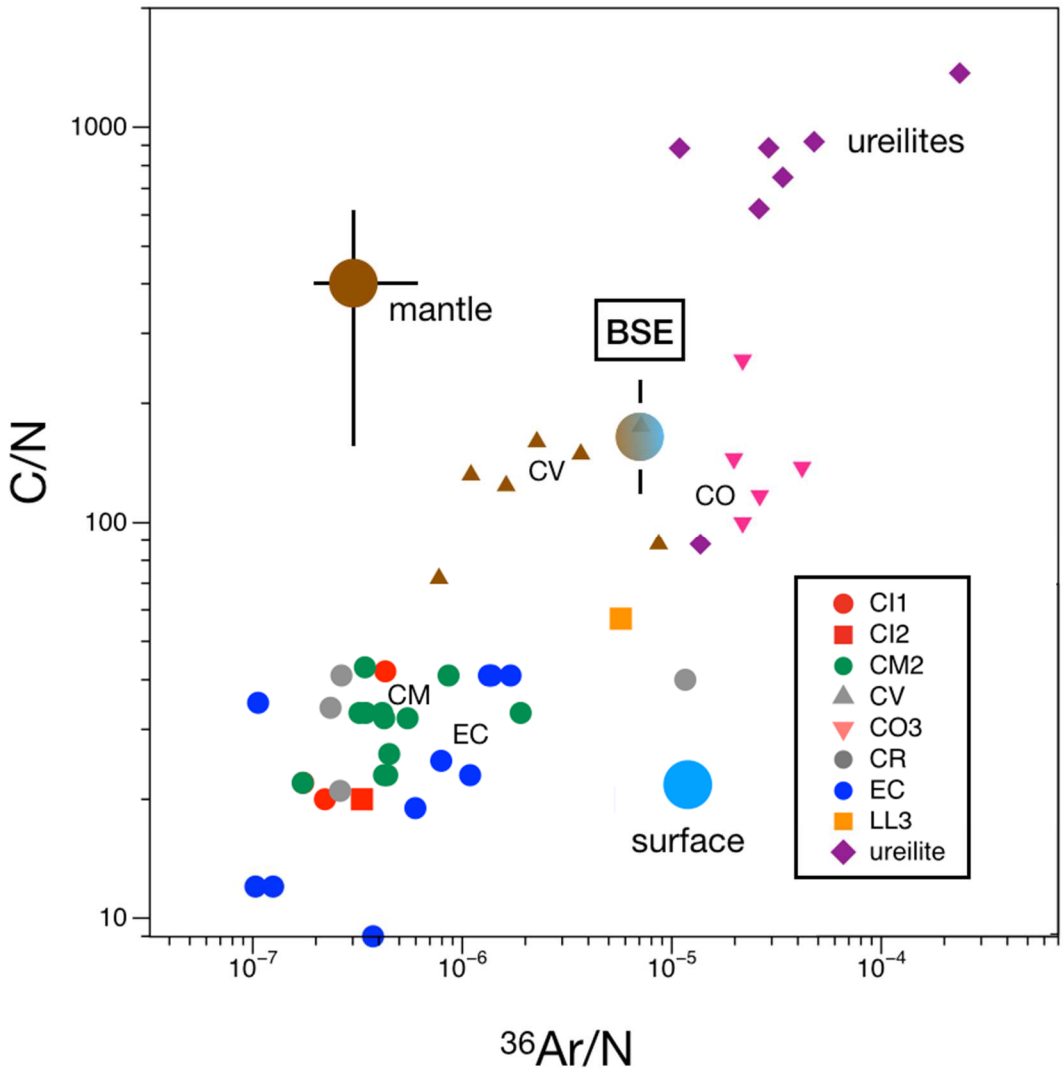

841

842

843 **Figure 5**: *C/N* versus $^{36}Ar/N$ for meteorites and terrestrial reservoirs (note the logarithmic

844 scale). See *Table 4* for terrestrial estimates, *Supplementary Table S1* for meteoritic data, and

845 Supplementary Fig. S5 for discussion of meteoritic data.

846

847

Alexander, C.M.O., Bowden, R., Fogel, M.L., Howard, K.T., Herd, C.D.K., Nittler, L.R., 2012. The provenances of asteroids, and their contributions to the volatile inventories of the terrestrial planets. Science 337, 721–3. doi:10.1126/science.1223474

Alexander, C.M.O., Howard, K.T., Bowden, R., Fogel, M.L., 2013. The classification of CM and CR chondrites using bulk H, C and N abundances and isotopic compositions. Geochim. Cosmochim. Acta 123, 244–260. doi:10.1016/j.gca.2013.05.019

Bischoff, A., Palme, H., Ash, R.D., Clayton, R.N., Schultz, L., Herpers, U., Stöffler, D., Grady, M.M., Pillinger, C.T., Spettel, B., Weber, H., Grund, T., Endreß, M., Weber, D., 1993. Paired Renazzo-type (CR) carbonaceous chondrites from the Sahara. Geochim. Cosmochim. Acta 57, 1587–1603. doi:10.1016/0016-7037(93)90014-N

Bogard, D.D., Clark, R.S., Keith, J.E., Reynolds, M.A., 1971. Noble gases and radionuclides in Lost City and other recently fallen meteorites. J. Geophys. Res. 76, 4076–4083. doi:10.1029/jb076i017p04076

Crabb, J., Anders, E., 1981. Noble gases in E-chondrites. Geochim. 45, 2443–2464.

Downes, H., Abernethy, F.A.J., Smith, C.L., Ross, A.J., Verchovsky, A.B., Grady, M.M., Jenniskens, P., Shaddad, M.H., 2015. Isotopic composition of carbon and nitrogen in ureilitic fragments of the Almahata Sitta meteorite. Meteorit. Planet. Sci. 50, 255–272. doi:10.1111/maps.12413

Eugster, O., Lorenzetti, S., Krähenbühl, U., Marti, K., 2007. Comparison of cosmic-ray exposure ages and trapped noble gases in chondrule and matrix samples of ordinary, enstatite, and carbonaceous chondrites. Meteorit. Planet. Sci. 42, 1351–1371. doi:10.1111/j.1945-5100.2007.tb00579.x

Göbel, R., Ott, U., Begemann, F., 1978. On trapped noble gases in ureilites. J. Geophys. Res. 83, 855. doi:10.1029/JB083iB02p00855

873 Grady, M.M., Verchovsky, A.B., Franchi, I.A., Wright, I.P., Pillinger, C.T., 2002. Light
874 element geochemistry of the Tagish Lake CI2 chondrite : Comparison with CI1 and CM2
875 meteorites. Meteorit. Planet. Sci. 37, 713–735.
876 Grady, M.M., Wright, I.P., Carr, L.P., Pillinger, C.T., 1986. Compositional differences in
877 enstatite chondrites based on carbon and nitrogen stable isotope measurements. Geochim.
878 Cosmochim. Acta 50, 2799–2813.
879 Grady, M.M., Wright, I.P., Swart, P.K., Rllinger, C.T., 1985. The carbon and nitrogen
880 isotopic composition of ureilites : implications for their genesis 49.
881 Kerridge, F., 1985. Carbon, hydrogen and nitrogen in carbonaceous chondrites: abundances
882 and isotopic compositions in bulk samples. Geochim. Cosmochim. Acta 49, 1707–1714.
883 Mazor, E., Heymann, D., Anders, E., 1970. Noble gases in carbonaceous chondrites. Geochim.
884 Cosmochim. Acta 34, 781–824.
885 Murty, S.V.S., Mahajan, R.R., Jenniskens, P., Shaddad, M.H., Eldien, B., 2010. Noble gases
886 and nitrogen in the Almahata Sitta ureilite. Meteorit. Planet. Sci. 45, 1751–1764.
887 doi:10.1111/j.1945-5100.2010.01095.x
888 Nakamura, T., Noguchi, T., Zolensky, M.E., Tanaka, M., 2003. Mineralogy and noble-gas
889 signatures of the carbonate-rich lithology of the Tagish Lake carbonaceous chondrite:
890 evidence for an accretionary breccia. Earth Planet. Sci. Lett. 207, 83–101.
891 doi:10.1016/S0012-821X(02)01127-5
892 Okazaki, R., Nagao, K., 2017. Title Primordial and cosmogenic noble gases in the Sutter's
893 Mill CM chondrite. Meteorit. Planet. Sci. 52, 669–689. doi:doi.org/10.1111/maps.12819
894 Ott U., Loehr H.P. and Begemann F. (1985) Trapped noble gases in 5 more ureilites and the
895 possible role of Q. Lunar Planet. Sci. **16**, 639-640.
896 Patzer, A., Schultz, L., 2001. Noble gases in enstatite chondrites I: Exposure ages, pairing,
897 and weathering effects. Meteorit. Planet. Sci. 36, 947–961. doi:10.1111/j.1945-

898 5100.2001.tb01932.x
899 Pearson, V.K., Sephton, M.A., Franchi, I.A., Gibson, J.M., Gilmour, I., 2006. Carbon and
900 nitrogen in carbonaceous chondrites: Elemental abundances and stable isotopic
901 compositions. Meteorit. Planet. Sci. 41, 1899–191